Realization of tunnel barriers for matter waves using spatial gaps

P. Cheiney[1,2], F. Damon[3,4], G. Condon[1,2], B. Georgeot[3,4] and D. Guéry-Odelin[1,2]

[1] *Université de Toulouse, UPS, Laboratoire Collisions Agrégats Réactivité, IRSAMC*
F-31062 Toulouse, France, EU
[2] *CNRS, UMR 5589 - F-31062 Toulouse, France, EU*
[3] *Université de Toulouse, UPS, Laboratoire de Physique Théorique, IRSAMC - F-31062 Toulouse, France, EU*
[4] *CNRS, UMR 5152 - F-31062 Toulouse, France, EU*

Abstract – We experimentally demonstrate the trapping of a propagating Bose-Einstein Condensate in a Bragg cavity produced by an attractive optical lattice with a smooth envelope. As a consequence of the envelope, the band gaps become position-dependent and act as mirrors of finite and velocity-dependent reflectivity. We directly observe both the oscillations of the wave packet bouncing in the cavity provided by these spatial gaps and the tunneling out for narrow classes of velocity. Synchronization of different classes of velocity can be achieved by proper shaping of the envelope. This technique can generate single or multiple tunnel barriers for matter waves with a tunable transmission probability, equivalent to a standard barrier of submicron size.

The tunneling effect is a cornerstone of quantum mechanics according to which a particle can penetrate and even pass through a classically impenetrable barrier. This behavior results from the wave nature of particles and is at work in many domains of physics including nuclear disintegration [1,2], quantum electronics [3,4], scanning tunneling microscope [5], tunnel ionization [6,7] and in various superconducting devices [8,9].

For cold atoms placed in optical lattices, the tunnel effect controls the coupling between adjacent wells and is therefore an essential parameter to build the band structure and describe the dynamics [7,10,11]. Recent experiments have demonstrated the possibility to control this coupling dynamically in amplitude and phase [12–15].

Realizing a thin enough single barrier enabling one to investigate atom tunneling dynamics remains very challenging. This has been realized so far in at least three different ways in the context of atomic Josephson physics using i) the combination of an optical lattice and a harmonic potential [16], ii) a strongly focussed far-off resonance blue-detuned laser [17] and iii) RF-dressed potentials [18].

The concept of the tunnel effect has been generalized to other kinds of space. The Landau-Zener transition between the energy bands of a lattice can be seen as a tunnel effect in quasi-momentum space [10]. Dynamical tunneling has been introduced to describe the tunneling between classically trapped regions in a regular phase space [19]. Its extension to a partially chaotic phase space, is referred to as chaos-assisted tunneling and has been observed using a deep and strongly modulated optical lattice [20,21]. The tunneling of magnetic flux across a superconducting wire has been recently observed [9].

In this letter, we realize a new kind of tunnel barrier in real space using position-dependent band gaps resulting from the smooth envelope of an optical lattice [22–25]. In this way, we can generate a Bragg cavity for matter waves with effective mirrors of tunable reflectivity, and directly observe the oscillations of a wave packet (provided by a Bose-Einstein condensate) inside such a cavity along with single tunneling events whenever the packet bounces off these effective mirrors.

We use an attractive lattice with Gaussian envelope resulting from the interference of two off-resonance and red-detuned Gaussian laser beams. An atom in such a lattice experiences a potential $U(x) = -U_0(x)\sin^2(\pi x/d)$, where $U_0(x) = U_0 \exp(-2x^2/w^2)$ accounts for the envelope, U_0
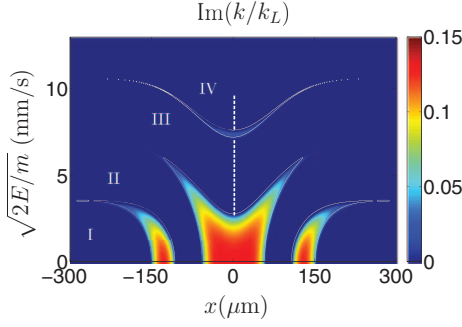
Fig. 1: (Color online) The color scale denotes the imaginary part of the Mathieu exponent k with the following lattice parameters: $U_0/E_L = 2.5$, $d = 650\,$nm and $w = 145\,\mu$m. Regions where $\mathrm{Im}(k) \neq 0$ correspond to evanescent waves. The roman numbers indicate the band index. The dashed line depicts the initial energy distribution (95% of the atoms).

is the maximum lattice depth, d the lattice spacing, and w the Gaussian envelope waist.

For an infinite optical lattice of constant depth U_0, the stationary Schrödinger equation is a Mathieu equation [26,27] whose solutions read

$$\Psi(x; E, U_0) = e^{ik(E)x} u_k(x; E, U_0), \qquad (1)$$

where u_k is a periodic function of period d and k is the Mathieu exponent. If the energy E corresponds to an allowed band of the Bloch diagram, k is real and corresponds to the pseudo-momentum of a Bloch state. When E lies in a gap, k acquires an imaginary part. The solution of the Mathieu equation is then an evanescent wave that decreases exponentially on a typical length scale $\Delta x_{\mathrm{tunnel}} = 1/\mathrm{Im}(k)$ and the real part remains on one edge of the Brillouin zone.

For a finite optical lattice with a space-dependent depth $U(x)$, the same solution locally holds within the assumption of a slowly varying envelope ($d \ll w$) and yields space-dependent wave vectors k. In fig. 1, we show the imaginary part of the Mathieu exponent as a function of position and square root of the energy for $U_0 = 2.5 E_L$ where $E_L = \hbar^2 k_L^2/2m$ with $k_L = 2\pi/d$ and m is the atom mass. Note that the energy is positive (relative to the continuum far from the attractive lattice) so that a reflection in this context has no classical counterpart and results from a pure quantum effect of matter wave interferences[1] [28]. The regions where $\mathrm{Im}(k) \neq 0$ define spatial gaps that separate the different allowed bands. The symmetry of the band structure originates from the symmetry of the Gaussian envelope.

According to this picture, the reflection on a gap corresponds to a Bragg reflection [29], while tunneling through the barrier provided by the spatial gaps is analogous to a Landau-Zener transition to a different band [30]. The

---

[1]The energy E coincides with the kinetic energy $mv_{\mathrm{inc}}^2/2$ where v_{inc} is the incoming velocity far from the lattice.
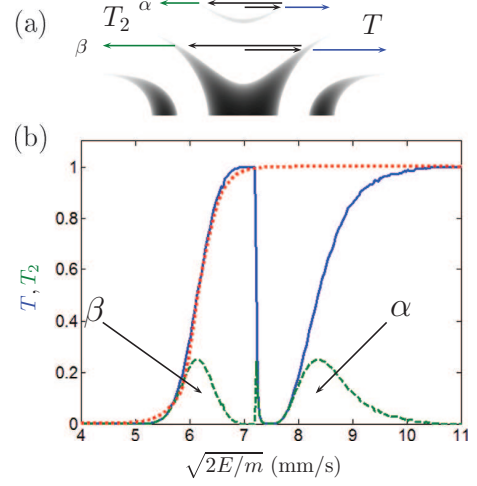

Fig. 2: (Color online) (a) Schematic of the evolution of the wave packet inside the lattice (see text). (b) Transmission probability of the wave packet. Solid (blue line): transmission probability given by eq. (2) through half of the lattice, the regions of reflection correspond to important band gaps. Dotted (red line): transmission probability through a repulsive Gaussian barrier of variance $\sigma = 387\,$nm. Dashed (green line): transmission probability to tunnel out of the lattice after one oscillation. The parameters of the lattice are identical to those of fig. 1.

same ingredients explain the macroscopic tunneling observed in a vertical lattice [31].

The transmission probability of a monochromatic wave with energy E through a single barrier can readily be calculated by integrating $\mathrm{Im}(k)$,

$$T(E) = \exp\left(\int -2\mathrm{Im}[k(x, E)]\mathrm{d}x\right), \qquad (2)$$

and is represented for our parameters as the (blue) solid line in fig. 2. The two regions where the transmission probability vanishes correspond to reflections on different spatial gaps. At the edge between regions of transmission and reflection, atoms have a high probability to tunnel through a spatial gap. It is instructive to fit this transmission probability with the one obtained from a repulsive Gaussian barrier. For the spatial gap β (see fig. 2(a)) that is $10\,\mu$m wide, we find the best agreement for a standard deviation of the Gaussian of $\sigma = 387\,$nm (see red dotted line in fig. 2(b)). It would be quite challenging to realize such a barrier directly by optical means since it requires to focus a blue-detuned laser of waist 2σ close to its diffraction limit inside a vacuum chamber.

In our experiment (see below), we initially load the atoms at the center of the lattice with an energy distribution that spreads over the third band and the bottom of the fourth band (see the vertical white dashed line in fig. 1) [25]. By energy conservation, the "trajectory" of an atom with a well-defined incident velocity remains on a horizontal line in the diagram of fig. 1 and may be split

on the spatial gaps because of a partial tunneling. Atoms at the bottom of the third band experience a large gap and are thus reflected with a probability close to one. They bounce back and forth quasi-indefinitely. Atoms loaded at the top of the band see essentially no gap and immediately leave the lattice. Between these two extreme cases, atoms have an intermediate tunneling probability and can leave the trap after one, or several oscillations. The (green) dashed line of fig. 2 represents the probability $T_2 = T(E)(1 - T(E))$ to bounce back on the first gap then tunnel out of the cavity at the symmetric position (see fig. 2(a)). It presents peaks at energies corresponding to tunneling probabilities $T \sim 0.5$. The outcoupling of these atoms can thus be unambiguously attributed to a single tunneling event.

We now turn to our experimental setup. We first produce a ^{87}Rb Bose-Einstein condensate of typically $3 \cdot 10^4$ atoms after 3.5 s of forced evaporation in a crossed dipole trap [28]. The trap consists of two red-detuned (1070 nm) laser beams: a horizontal beam later used as a guide in the lattice direction x and a dimple beam. During the evaporation, we use the spin-distillation technique to prepare atoms in $|F = 1, m_F = 1\rangle$ [32]. Once the Bose-Einstein condensate is formed, the power of the dimple beam is reduced by a factor ~ 20 over 100 ms to decrease the chemical potential [33]. The condensate is subsequently released in the horizontal guide by switching off abruptly the dimple beam. The guide confines the transverse degrees of freedom and the lattice is along the guide axis. This configuration avoids couplings between the longitudinal and transverse degrees of freedom and therefore ensures a quasi–one-dimensional dynamics. Our protocol yields a wave packet with a relatively low-velocity dispersion $\Delta v = 1.9$ mm/s dictated here by the strength of the interactions combined with our trap decompression. In the course of the propagation, interactions become rapidly negligible.

The optical lattice is produced at the intersection of two red-detuned laser beams with a wavelength $\lambda_L = 840$ nm and a waist $\tilde{w} = 110 \, \mu$m crossing at an angle $\theta = 81°$ at the initial position of the wave packet. The resulting lattice spacing is $d = \lambda_L/[2\sin(\theta/2)] \simeq 650$ nm, and the envelope waist $w = \tilde{w}/\cos(\theta/2) = 145 \, \mu$m. The lattice detuning is large enough so that spontaneous emission is negligible over the duration of the experiment. To calibrate *in situ* the potential depth U_0, we use a Kapitza-Dirac diffraction [34].

The wave packet is set into motion at a mean velocity of $\bar{v} = 9.4$ mm/s by applying a magnetic-field gradient of 14 G/cm along the guide axis during 4 ms. We then linearly ramp the lattice power up to $U_0 = 2.5E_L$ in 1 ms. This time scale has been chosen to ensure an adiabatic increase of the lattice depth. This means that the intensity is ramped up such that [35,36]

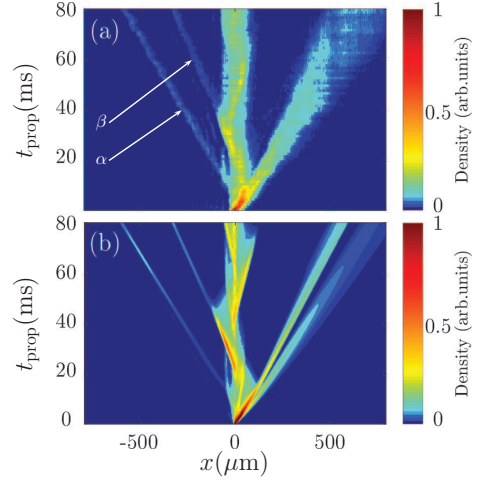$$\frac{dU_0}{dt} \ll \frac{E_L}{\hbar} \Delta E_k^2/E_L^2, \tag{3}$$

Fig. 3: (Color online) (a) Measured density distribution of the wave packet for different propagation times. Each horizontal line is the average of 4 images integrated along the transverse direction. (b) Direct numerical integration of the Schrödinger equation for a wave packet whose velocity distribution matches the experimental one.

where ΔE_k is the energy difference between the initial state $|n, k\rangle$ and the first excitable state $|n', k\rangle$ on the adjacent band.

According to our numerical simulations, this is already verified for ramping times as short as $100 \, \mu$s, except for a small number of atoms whose pseudo-momentums lie close to the Brillouin zone edge and for which $\Delta E_k = 0$ at the beginning of the adiabatic loading[2]. The pseudo-momentum remains constant in the adiabatic loading process. This allows us to determine the final energy distribution of the wave packet (see the vertical white dashed line in fig. 1) [25]. We then let the wave packet propagate for different times before imaging the atoms *in situ*.

Figure 3(a) shows the measured atomic density along the guide during the propagation. Each horizontal line is the average of four images integrated along the transverse direction. In this experiment, all atoms are initially launched toward the right side of the lattice. For the sake of comparison, fig. 3(b) is the result of the numerical integration of the Schrödinger equation using a split-Fourier algorithm with a wave packet whose characteristics match the experimental ones without any adjustable parameter. Three effects can be noticed: i) part of the wave packet immediately leaves the lattice, it corresponds to velocity classes ($6.7 < v < 7.2$ and $v > 9.5$ mm/s) that do not encounter a significant band gap; ii) a periodic oscillations inside the lattice can be clearly observed; iii) in the direction opposite to the initial velocity we observe the

---

[2]These atoms correspond to the extremely narrow peak at 7.3 mm/s observed in the transmission in the simulation (see fig. 4(a)). They are not visible in the experiment.
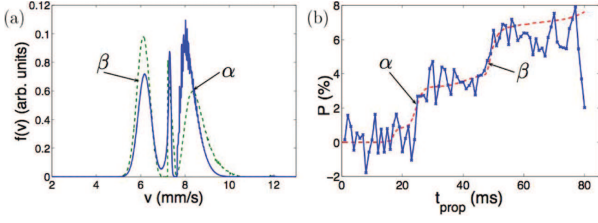
Fig. 4: (Color online) (a) Calculated velocity distribution of atoms that leave the lattice after one oscillation using the band model (green dashed line) and the full numerical integration (blue solid line). (b) Proportion of atoms on the left side of the lattice. Experimental results (blue solid line). The red dashed line is the numerical integration result without any adjustable parameters.

emission from the left side of the lattice of two atomic packets denoted α and β. They leave the lattice by tunneling through a spatial gap and then propagate freely. Their transmission probabilities have been represented in fig. 2(b).

The oscillations have a period of approximately 50 ms and appear as regular spines. They are washed out after a few oscillations. Both of these effects are the consequence of the important initial energy dispersion. The spines structures are caustics formed by the addition in these regions of the trajectories associated with each energy component. The most energetic atoms travel faster inside the lattice but face the spatial gap at a larger distance from the center for a given spatial gap cavity (see fig. 1). For a Gaussian envelope, the second effect turns out to be larger so that the period of oscillation increases with energy. The washing out of the oscillations at long time results from the progressive dephasing of the different energy components.

Figure 4(b) shows the measured (data of fig. 3(a)) and calculated (using the full integration) proportion of atoms on the left side of the lattice at a distance larger than $150\,\mu$m from the center as a function of time. It displays two steps that represent each about 3% of the total number of atoms and correspond to the two tunneling events observed in fig. 3. Atoms on the fourth band generate the first tunnel packet (α) in a direction opposite to the launching velocity direction at $t_{\mathrm{prop}} \simeq 25\,$ms. Atoms in the middle of the third band experience a larger cavity and give rise to the second observed tunnel packet (β) at $t_{\mathrm{prop}} \simeq 50\,$ms.

The measured mean velocities of these narrow wave packets are 7.9 ± 0.1 and $5.9 \pm 0.1\,$mm/s, respectively. These atoms have performed half an oscillation before leaving the lattice, the atom number and energy distributions can thus be calculated by integrating the probability T_2 over the initial energy distribution. We find that the transmissions peaks α and β depicted in fig. 2 (dashed line) contain, respectively, 3.2% and 3.0% of the total number of atoms. Figure 4(a) shows the velocity

distribution on the left side using the local bands model (green dashed line) and the direct integration (blue solid line). The calculated mean velocities of the two peaks are 5.9 and 8.3 mm/s, respectively, using the band model calculation and 6.1 and 8.1 mm/s using the numerical integration in good agreement with the measured values. The two r.m.s velocity dispersions are similar and in the range $\Delta v \simeq 250\,\mu$m/s. This selectivity is as high as the one provided by Bragg scattering or velocity-selective Raman transitions [20,37–39] and does not require any specific internal state configuration.

Surprisingly at first sight, the wave packets that have tunneled out from the spatial gaps α and β do not seem to expand significantly even after 80 ms of propagation. Actually, the full numerical integration indicates that the wave packets are focused at a finite time ($t_{\mathrm{prop}} \simeq 65\,$ms for the packet α). This is due once again to the dispersion of the oscillation periods: the slow atoms have a shorter period and tunnel before the rapid ones. Outside the lattice this results in a chirped pulse with the high frequencies at the back. High-velocity components then catch up with the slow ones at a finite time. This effect hinders the direct measurement of the velocity dispersion by a time of flight. The dephasing of the different energy components may appear as a limitation of the Bragg cavity device, it enlarges the initial width of the tunneled packets and reduces the number of visible oscillations. Nevertheless, it is possible to circumvent this apparent limitation by keeping the different components in phase with a proper shaping of the envelope.

This shaping consists in adjusting the size of the cavity to compensate exactly for the change in group velocity. In the following, we demonstrate the optimization of the envelope shape using the *ansatz* $U_0(x) = -U_0 \exp(-2x^2/w^2)(1 + x^2/D^2)$, where D is a free parameter. Such an envelope can be realized using holographic plates. This *ansatz* keeps the symmetry of the Gaussian but has steeper spatial gaps if $D > 0$. Because of the caustic effect, it is difficult to define an oscillation period using the numerical integration. Thereby, we have performed this optimization using a semiclassical model [40]. In such an approach, the particle motion on a given local Bloch band n is described by the combined evolution of the wave packet position and of its mean pseudo-momentum k:

$$\dot{x} = \frac{1}{\hbar}\frac{\partial E_n}{\partial k} \qquad \text{and} \qquad \dot{k} = -\frac{1}{\hbar}\frac{\partial E_n}{\partial x}. \qquad (4)$$

The optimization is performed by cancelling out the first-order variation of the oscillation period with energy for trajectories with nearby initial pseudo-momentum[3]. For our parameters, we find $D = 0.75w = 112\,\mu$m. In fig. 5, we compare the results for a packet of velocity dispersion $\Delta v = 1.2\,$mm/s for the semiclassical approach and the

_____

[3]It is possible to extend the *ansatz* to higher order to cancel out the second derivative of the oscillation period; however the resulting potentials have a much more complicated shape.
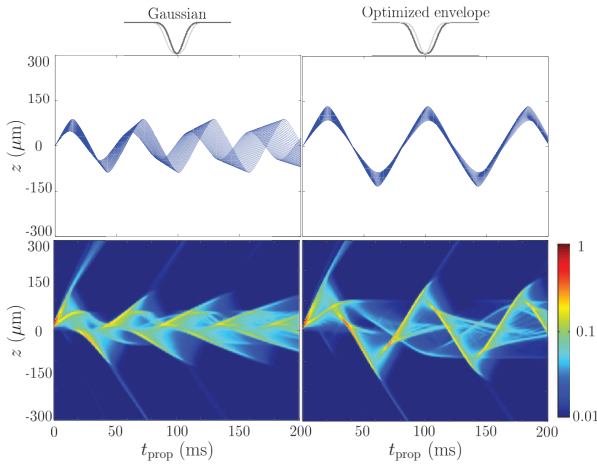
Fig. 5: (Color online) Envelope engineering. Semiclassical trajectories (upper panel) and full numerical integration (lower panel) of the wave packet dynamics in (left) the Gaussian envelope lattice and in (right) the lattice with an optimized envelope (see text); the color scale is logarithmic. Parameters: initial velocity spread $\Delta v = 1.2\,\text{mm/s}$, $D = 0.75\,w = 112\,\mu\text{m}$.

full numerical integration with and without the optimization. The optimization greatly reduces the blurring of the oscillations, and therefore all velocity components tunnel at the same time, generating a train of nearly identical matter wave pulses, *i.e.* a mode-locked atom laser.

In conclusion, we have demonstrated that spatial gaps resulting from an inhomogeneous envelope of a lattice produce barriers with a probability transmission equivalent to thin real barriers of a few hundreds of nm. They open new perspectives for single tunnel barrier physics including time-modulated tunnel barrier, many-body wave functions (such as solitons) tunneling [41–43], Josephson-like experiments [17,18]. This system is also of interest for multiple barriers configurations including cavity or Anderson localization investigation in real space [44,45]. It can be readily generalized to higher dimensions and may be used as a test bed for semiclassical approaches of tunneling in 2D [46].

$$* * *$$

REFERENCES

[1] Gamow G., *Z. Phys.*, **51** (1928) 204.
[2] Gurney R. W. and Condon E. U., *Phys. Rev.*, **33** (1929) 127.
[3] Esaki L., *Phys. Rev.*, **109** (1958) 603.
[4] Esaki L., *Rev. Mod. Phys.*, **46** (1974) 237.
[5] Binnig G. and Rohrer H., *Rev. Mod. Phys.*, **59** (1987) 615.
[6] Krausz F. and Ivanov M., *Rev. Mod. Phys.*, **81** (2009) 163.
[7] Cohen-Tannouji C. and Guéry-Odelin D., *Advanves in Atomic Physics: An Overview* (World Scientific, Singapore) 2011.
[8] Josephson B., *Phys. Lett.*, **1** (1962) 251.
[9] Astafiev O. V., Ioffe L. B., Kafanov S., Pashkin Y. A., Arutyunov K. Y., Shahar D., Cohen O. and Tsai J. S., *Nature*, **484** (2012) 355.
[10] Morsch O. and Oberthaler M., *Rev. Mod. Phys.*, **78** (2006) 179.
[11] Bloch I., Dalibard J. and Zwerger W., *Rev. Mod. Phys.*, **80** (2008) 885.
[12] Eckardt A., Weiss C. and Holthaus M., *Phys. Rev. Lett.*, **95** (2005) 260404.
[13] Lignier H., Sias C., Ciampini D., Singh Y., Zenesini A., Morsch O. and Arimondo E., *Phys. Rev. Lett.*, **99** (2007) 220403.
[14] Kierig E., Schnorrberger U., Schietinger A., Tomkovic J. and Oberthaler M., *Phys. Rev. Lett.*, **100** (2008) 190405.
[15] Struck J., Ölschläger C., Le Targat R., Soltan-Panahi P., Eckardt A., Lewenstein M., Windpassinger P. and Sengstock K., *Science*, **333** (2011) 996.
[16] Albiez M., Gati R., Fölling J., Hunsmann S., Cristiani M. and Oberthaler M., *Phys. Rev. Lett.*, **95** (2005) 010402.
[17] Levy S., Lahoud E., Shomroni I. and Steinhauer J., *Nature*, **449** (2007) 579.
[18] Betz T., Manz S., Bücker R., Berrada T., Koller C., Kazakov G., Mazets I. E., Stimming H.-P., Perrin A., Schumm T. and Schmiedmayer J., *Phys. Rev. Lett.*, **106** (2011) 020407.
[19] Davis M. J. and Heller E. J., *J. Chem. Phys.*, **75** (1981) 246.
[20] Steck D. A., Oskay W. H. and Raizen M., *Science*, **293** (2001) 274.
[21] Haffner H., Browaeys A., Heckenberg N. R., Helmerson K., McKenzie C., Milburn G. J., Phillips W. D., Rolston S. L., Rubinsztein-Dunlop H. and Upcroft B., *Nature*, **412** (2001) 52.
[22] Santos L. and Roso L., *Phys. Rev. A*, **60** (1999) 2312.
[23] Carusotto I., Embriaco D. and La Rocca G. C., *Phys. Rev. A*, **65** (2002) 053611.
[24] Carusotto I. and La Rocca G. C., *Phys. Rev. Lett.*, **84** (2000) 399.
[25] Lauber T., Massignan P., Birkl G. and Sanpera A., *J. Phys. B: At. Mol. Opt. Phys.*, **44** (2011) 065301.
[26] Magnus W. and Winkler S., *Hill's Equation* (John Willey and Sons, New York) 1947.
[27] Sträng J. E., *Acad. R. Belg. Bull. Cl. Sci.*, **6** (2005) 269.
[28] Fabre C. M., Cheiney P., Gattobigio G. L., Vermersch F., Faure S., Mathevet R., Lahaye T. and Guéry-Odelin D., *Phys. Rev. Lett.*, **107** (2011) 230401.
[29] Ben Dahan M., Peik E., Reichel J., Castin Y. and Salomon C., *Phys. Rev. Lett.*, **76** (1996) 4508.

[30] Zener C., *Proc. R. Soc. London, Ser. A*, **137** (1932) 696.

[31] Anderson B. P. and Kasevich M. A., *Science*, **282** (1998) 1686.

[32] Gattobigio G. L., Couvert A., Jeppesen M., Mathevet R. and Guéry-Odelin D., *Phys. Rev. A*, **80** (2009) 041605(R).

[33] Vermersch F., Fabre C. M., Cheiney P., Gattobigio G. L., Mathevet R. and Guéry-Odelin D., *Phys. Rev. A*, **84** (2011) 043618.

[34] Ovchinnikov Y. B., Müller J. H., Doery M. R., Vredenbregt E. J. D., Helmerson K., Rolston S. L. and Phillips W. D., *Phys. Rev. Lett.*, **83** (1999) 284.

[35] Hecker Denschlag J., Simsarian J. E., Haffner H., McKenzie C., Browaeys A., Cho D., Helmerson K., Rolston S. L. and Phillips W. D., *J. Phys. B: At. Mol. Opt. Phys.*, **35** (2002) 3095.

[36] Schiff L., *Quantum Mechanics* (McGraw-Hill, New York) 1968.

[37] Kozuma M., Deng L., Hagley E. W., Wen J., Lutwak R., Helmerson K., Rolston S. L. and Phillips W. D., *Phys. Rev. Lett.*, **82** (1999) 871.

[38] Kasevich M. and Chu S., *Phys. Rev. Lett.*, **69** (1992) 1741.

[39] Battesti R., Cladé P., Guellati-Khélifa S., Schwob C., Grémaud B., Nez F., Julien L. and Biraben F., *Phys. Rev. Lett.*, **92** (2004) 253001.

[40] Cheiney P., Fabre C., Vermersch F., Gattobigio G. L., Mathevet R., Lahaye T. and Guéry-Odelin D., *Phys. Rev. A*, **87** (2013) 013623.

[41] del Campo A., Delgado F., Garcia-Calderon G., Muga G. and Raizen M., *Phys. Rev. A*, **74** (2006) 013605.

[42] Ahufinger V., Malomed B. A., Birkl G., Corbalán R. and Sanpera A., *Phys. Rev. A*, **78** (2008) 013608.

[43] Hansen S. D., Nygaard N. and Molmer K., http://arxiv.org/abs/1210.1681.

[44] Billy J., Josse V., Zuo Z., Bernard A., Hambrecht B., Lugan P., Clement D., Sanchez-Palencia L., Bouyer P. and Aspect A., *Nature*, **453** (2008) 891.

[45] Roati G., D'Errico C., Fallani L., Fattori M., Fort C., Zaccanti M., Modugno G., Modugno M. and Inguscio M., *Nature*, **453** (2008) 895.

[46] Keshavamurthy S. and Schlagheck P., *Dynamical Tunneling: Theory and Experiment* (CRC Press, Singapore) 2011.